Analysis of the modulation mechanisms of the electric field and breakdown performance in AlGaN/GaN HEMT with a T-shaped field-plate*

Wei Mao(毛维), Ju-Sheng Fan(范举胜), Ming Du(杜鸣)†, Jin-Feng Zhang(张金风), Xue-Feng Zheng(郑雪峰), Chong Wang(王冲), Xiao-Hua Ma(马晓华), Jin-Cheng Zhang(张进成), and Yue Hao(郝跃)

Key Laboratory of Ministry of Education for Wide Band-Gap Semiconductor Materials and Devices, School of Microelectronics, Xidian University, Xi'an 710071, *China*

(Received 15 August 2016; revised manuscript received 16 October 2016; published online 15 November 2016)

A novel AlGaN/GaN high electron mobility transistor (HEMT) with a source-connected T-shaped field-plate (ST-FP HEMT) is proposed for the first time in this paper. The source-connected T-shaped field-plate (ST-FP) is composed of a source-connected field-plate (S-FP) and a trench metal. The physical intrinsic mechanisms of the ST-FP to improve the breakdown voltage and the FP efficiency and to modulate the distributions of channel electric field and potential are studied in detail by means of two-dimensional numerical simulations with Silvaco-ATLAS. A comparison to the HEMT and the HEMT with an S-FP (S-FP HEMT) shows that the ST-FP HEMT could achieve a broader and more uniform channel electric field distribution with the help of a trench metal, which could increase the breakdown voltage and the FP efficiency remarkably. In addition, the relationship between the structure of the ST-FP, the channel electric field, the breakdown voltage as well as the FP efficiency in ST-FP HEMT is analyzed. These results could open up a new effective method to fabricate high voltage power devices for the power electronic applications.

Keywords: AlGaN/GaN HEMT, source-connected T-shaped field-plate, breakdown voltage, FP efficiency

PACS: 73.40.Kp, 85.30.Tv, 85.30.De **DOI:** 10.1088/1674-1056/25/12/127305

1. Introduction

If the successful development of GaN-based material could be considered as a vital catalyst for the invention of GaN-based high electron mobility transistor (HEMT), the field-plate (FP) technology could also be considered as one of the most prominent catalysts for significantly improving the power performance of HEMTs so as to satisfy more and more actual requirements in recent power applications. With the excellent ability of these FP techniques to effectively extend the depletion region and replace a single-peak electric field with several peaks,[1] the electric field distribution could be uniformed, the device breakdown performance and other relevant reliability performance, such as trapping effect,[2,3] inverse piezoelectric effect[4,5] could be improved. So far, various studies on the GaN-based HEMTs with different FP structures have been reported,[6–18] of which it may be one of the important focuses to improve the device breakdown voltage without increasing device dimension. Therefore, it could be concluded, to a great extent, that in order to fabricate a device with high breakdown voltage and little degradation of its other performances, it may be an effective and valuable method to raise the ability of the FP per unit length to enhance the breakdown voltage as much as possible, which deserves to be explored further.

In this paper, a novel AlGaN/GaN HEMT with a source-connected T-shaped field-plate (ST-FP HEMT) is presented for the purpose of a better breakdown enhancement and a better ability of the FP per unit length to increase the breakdown voltage. Systematic simulations of physical mechanism in ST-FP HEMT, relating to the improvement of the breakdown capability together with the ST-FP modulation effects on the channel electric field and potential distributions, are conducted in detail with Silvaco-ATLAS. In addition, the optimization methods, the relationship between the structure of the ST-FP, the breakdown voltage as well as the FP efficiency in ST-FP HEMT are achieved on the basis of the simulation researches. These research results could provide a valuable guideline for reducing the device design complexity and simplifying the actual manufacture processings of the ST-FP HEMT.

2. Device structures and simulation models

Figure 1 shows the schematics of the S-FP HEMT and the proposed ST-FP HEMT. The HEMT is not shown because of its same structure as that of S-FP HEMT except for none FP. As shown in the figure, the ST-FP is characterized by an S-FP and a trench metal. With the exception of the

*Project supported by the National Natural Science Foundation of China (Grant Nos. 61574112, 61334002, 61306017, 61474091, and 61574110) and the Natural Science Basic Research Plan in Shaanxi Province, China (Grant No. 605119425012).

†Corresponding author. E-mail: duming@mail.xidian.edu.cn

© 2016 Chinese Physical Society and IOP Publishing Ltd

FP structure, all the devices in this paper have the same device structure, which is similar to that used in Ref. [9]. A 3-μm unintentionally doped (UID) GaN buffer layer and a 30-nm UID $Al_{0.25}Ga_{0.75}N$ barrier layer are used. And the gate–source spacing, the gate length, and the gate–drain spacing are 1.5 μm, 1.5 μm, and 10 μm, respectively. The same effective FP length L_{FP} in S-FP HEMT and ST-FP HEMT is used. Silicon nitride passivation is used and the thickness under the FP is defined as T_{SiN}. L_{GT} is the distance from the gate to the trench. L_{TF} is the distance between the trench and the drain side of the ST-FP. The trench depth and width are denoted with T_D and L_T, respectively.

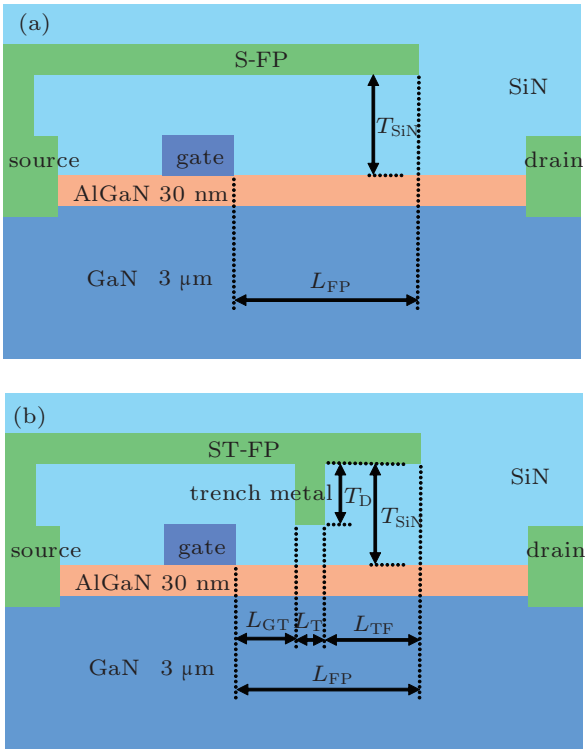


Fig. 1. (color online) Schematics of (a) S-FP HEMT and (b) ST-FP HEMT.

The simulations are performed with Silvaco-ATLAS and the main device model is similar to that in our early researches.[18,19] The background doping concentrations in the AlGaN layer and the GaN layer are both assumed to be 1×10^{15} cm^{-3}. The positive charges with a density of 1×10^{13} cm^{-2} are located along the AlGaN/GaN heterojunction to model the polarization effect, which is based on the experimental result of the approximate charge neutrality at the AlGaN/passivation layer interface.[20] Two kinds of deep traps are considered, of which the energy level and the density for the deep acceptor trap are $E_C - 2.85$ eV and 1×10^{17} cm^{-3} respectively, and those for the deep donor trap are $E_C - 0.5$ eV and 2×10^{17} cm^{-3}. The simulations about the breakdown performance are carried out with the gate biased at -6 V. And the breakdown voltage V_{BR} is defined as the drain voltage where the peak electric field in the channel reaches a GaN breakdown field of 3 MV/cm, whose breakdown criterion has been successfully implemented in our early researches.[18,19,21]

3. Results and discussion

In order to evaluate the ability of FP to improve the breakdown voltage reasonably, the FP efficiency η,[22] defined as a ratio of the increment of the breakdown voltage V_{BR} to the total effective FP length L_{FP}, is utilized in this paper. Figure 2 shows the relationship between the L_{FP} of S-FP and the breakdown voltage V_{BR} as well as the FP efficiency η in S-FP HEMT. In Fig. 2, each V_{BR} is approximately the maximum breakdown voltage for a given L_{FP}, which is obtained by optimizing the passivation thickness T_{SiN} in Fig. 1(a). It can be observed that the breakdown voltage increases while the FP efficiency decreases with the increase of the L_{FP}. And when the L_{FP} is beyond 5 μm, the increment of the V_{BR} with the L_{FP} is very small, corresponding to a small change of η. This phenomenon is in accordance with that in Ref. [6]. And the simulated V_{BR} of 475 V for an S-FP HEMT with $L_{FP} = 5$ μm in this paper is very close to the experimental data of 470 V for an S-FP HEMT with the same L_{FP} in Ref. [9]. These above indicate a good validity of our device model.

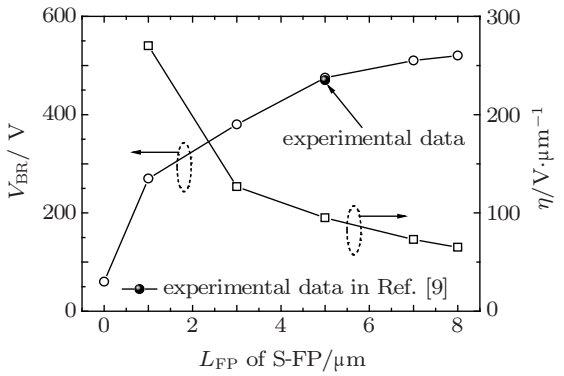


Fig. 2. Relationship between the L_{FP} of S-FP and the breakdown voltage V_{BR} as well as the FP efficiency η in S-FP HEMT.

Figure 3 shows the nearly optimized channel electric field distributions for the HEMT and four S-FP HEMTs with different values of L_{FP}. And the area beneath the contour of each electric field distribution in Fig. 3, could be used to estimate the V_{BR} of each device approximately. The channel electric field distributions away from the left edge of the gate or the FP are very small, thus they are not shown in Fig. 3. As can be seen, the V_{BR} of HEMT is only 60 V, with only one electric field peak near the gate edge. And it is evident that two nearly equal electric field peaks are formed at the right edge of the gate and the right edge of the S-FP in each S-FP HEMT, indicating an effective modulation of electric field with the S-FP at higher breakdown voltage. In addition, with the increase of L_{FP}, the V_{BR} of S-FP HEMT increases and the electric field peak near the right edge of the S-FP shifts toward the drain. And when the $L_{FP} > 5$ μm, the increment of the area beneath

the contour of the electric field distribution is very small, leading to a small increment of the V_{BR} and a small decrement of the η. These results are consistent with the analyses in Fig. 2.

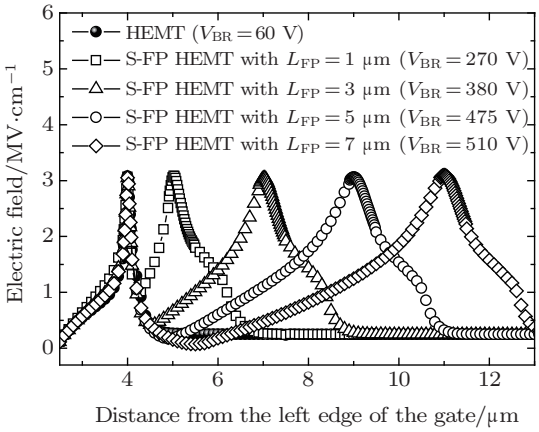


Fig. 3. Nearly optimized channel electric field distributions in HEMT and four S-FP HEMTs.

Careful observations of Fig. 3 could reveal that the value of the electric field between the two electric field peaks in each S-FP HEMT drops and the range of this low electric field is enlarged with the increase of L_{FP}. This indicates that a considerable part of the S-FP between the gate and the drain edge of the FP, especially for a long S-FP, does not really play an effective role in modulating the channel electric field. Thus, in order to enhance the modulation ability of the S-FP, it is full of significance to take some measures to improve the electric field distribution beneath the S-FP, of which the ST-FP HEMT is a kind of structure with great potential, as illustrated in Fig. 1(b) and Fig. 4.

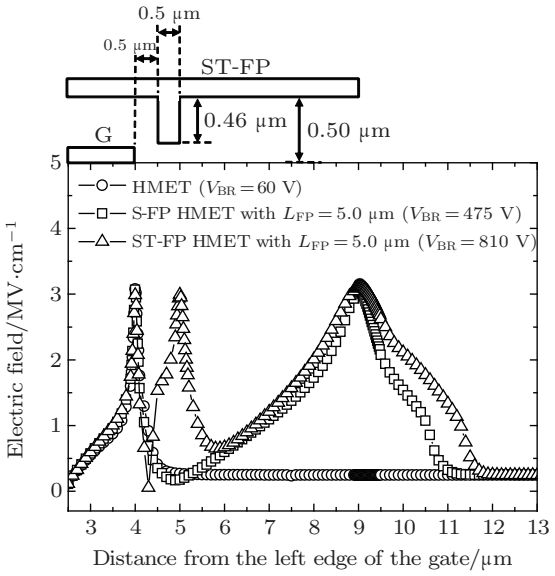


Fig. 4. Nearly optimized channel electric field distributions for the HEMT, the S-FP HEMT, and the ST-FP HEMT.

Figure 4 shows the nearly optimized channel electric field distributions beneath the field-plate or around the gate for the HEMT, the S-FP HEMT with an S-FP of $L_{FP} = 5$ μm and an ST-FP HEMT with an ST-FP of $L_{FP} = 5$ μm. The optimal T_{SiN} in the S-FP HEMT is 0.28 μm. And the optimal structure parameters of the ST-FP HEMT is achieved by optimizing the T_D and T_{SiN} for given $L_{GT} = 0.5$ μm and $L_T = 0.5$ μm. The optimal T_D and T_{SiN} are 0.46 μm and 0.5 μm, respectively. It is clear that a new electric field peak beneath the FP is formed in the ST-FP HEMT. And a broad electric field distribution near the drain edge of the FP in the ST-FP HEMT channel is obtained compared with that in the S-FP HEMT. This leads to a high V_{BR} of 810 V and a high η of 150 V/μm in the ST-FP HEMT, which exhibits a remarkable improvement compared with a V_{BR} of 475 V and an η of 83 V/μm in the S-FP HEMT.

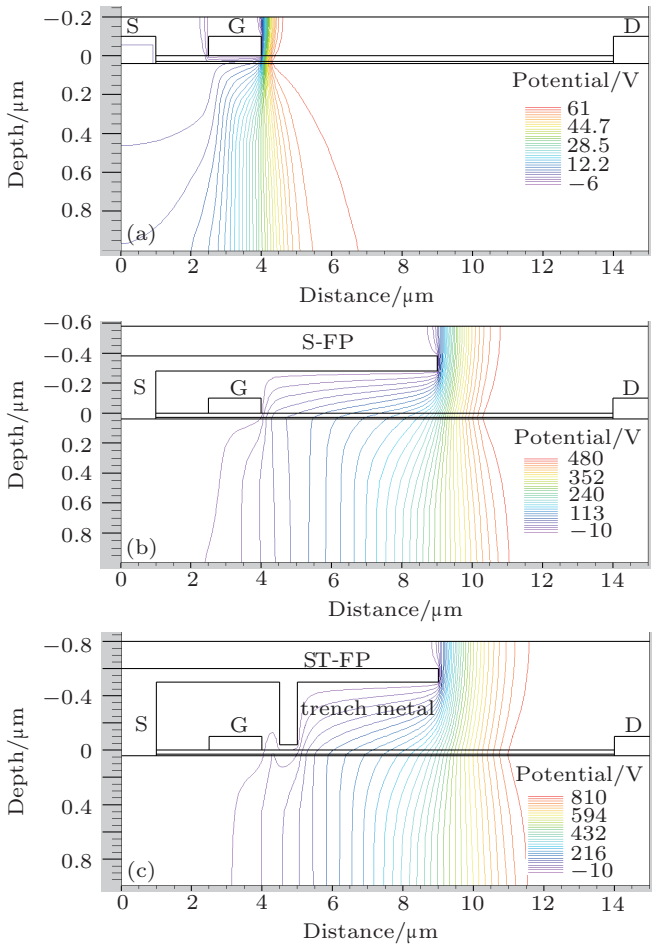


Fig. 5. (color online) Potential distributions in (a) HEMT, (b) S-FP HEMT, (c) ST-FP HEMT.

In order to get a physical insight into the essential mechanism of the modulation of the ST-FP, the potential distributions at off-state corresponding to the three devices in Fig. 4 are investigated as shown in Fig. 5. It can be observed that most of potential lines crowds around the drain side of the gate in HEMT, indicating a high electric field peak could be formed, which is in accord with the result in Fig. 4. And for the S-FP HEMT with an L_{FP} of 5 μm, the high potential line density appears at two positions: one is located at the drain side of the gate and the other at the drain side of the S-FP. This is attributed to the modulation effect of the S-FP, resulting in two electric field peaks in S-FP HEMTs. For the ST-FP HEMT,

a more uniform distribution of potential lines is observed and three high potential line density areas are formed at the gate edge, the trench edge and ST-FP edge, which shows an excellent and effective modulation of potential lines. Thus, a more uniform distribution of electric field as well as an outstanding blocking capability could be obtained in the ST-FP HEMT.

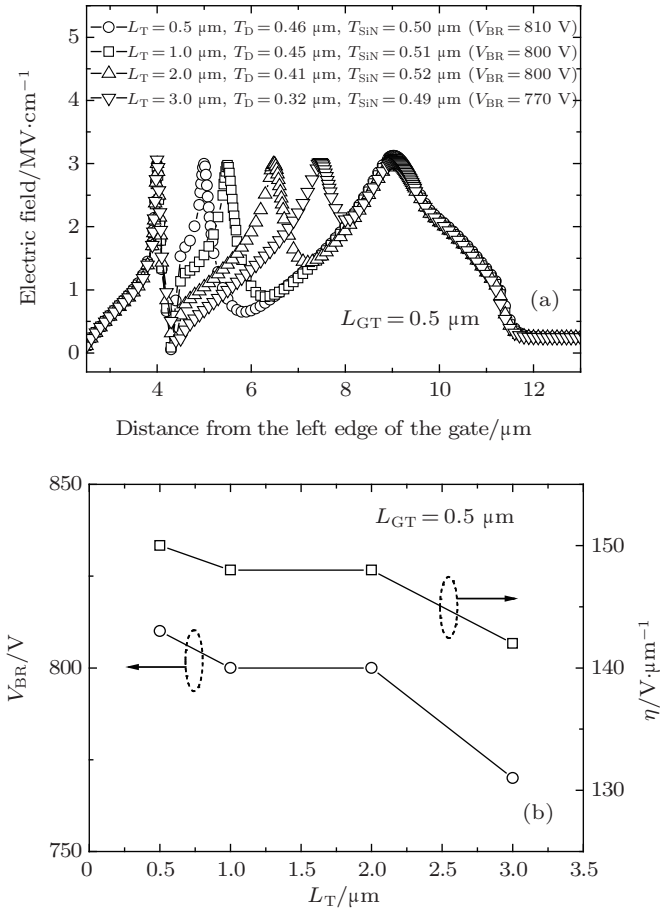


Fig. 6. (a) Electric field distributions along the channel and (b) relationship between the L_T, V_{BR} as well as η for ST-FP HEMTs with different values of L_T.

In the ST-FP HEMT, there are many structure parameters of the ST-FP which are needed to be considered during the device optimization. And each parameter may influence the breakdown voltage and the FP efficiency. Here, we take the L_T and the L_{GT} for example. For the purpose of illustration, the effects of the L_T and the L_{GT} in the ST-FP HEMT on the electric field distribution, V_{BR} as well as η are shown in Fig. 6 and Fig. 7, respectively. For devices with a fixed L_{GT} of 0.5 μm and each case of L_T in Fig. 6 and for devices with a fixed L_T of 0.5 μm and each case of L_{GT} in Fig. 7, they are all optimized to obtain the maximum V_{BR} by optimizing the T_D and T_{SiN}. As shown in Fig. 6, with increasing L_T, the electric field peaks near the drain side of the trench shift toward the drain, and the V_{BR} only shows a slight decrease, resulting in a slight drop of η. This indicates that the V_{BR} and η are both weak functions of L_T. When the trench width L_T is set to be 0.5 μm, the V_{BR} and η show strong functions of L_{GT} in Fig. 7. The smaller the L_{GT}, the greater the V_{BR} and η are. Besides, it could be found that the T_D is always a little smaller than the T_{SiN} in both figures. Based on these analyses, the optimization procedure of the ST-FP HEMT could be extracted. During the optimization, first, we could choose a proper trench width L_T according to the actual fabrication processing condition. And then for different given gate–trench spacings L_{GT}, the T_D and T_{SiN} are optimized to achieve the target breakdown voltage.

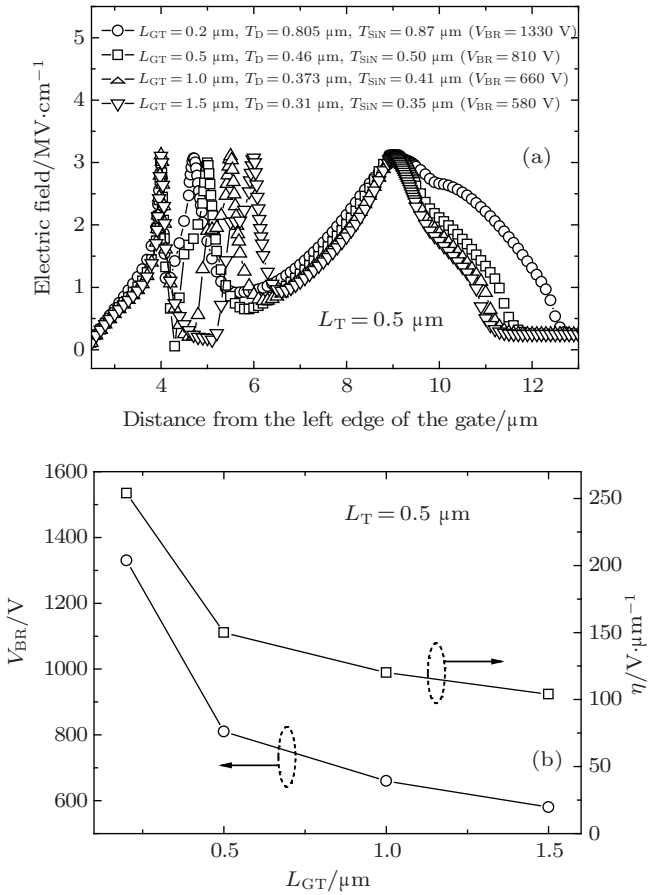


Fig. 7. ST-FP HEMT with different L_{GT}, (a) Electric field distributions along the channel and (b) relationship between the L_{GT}, V_{BR} as well as η for ST-FP HEMTs with different values of L_{GT}.

4. Conclusions

The off-state breakdown performance of the ST-FP HEMT with an ST-FP is investigated in this paper. With the help of two-dimensional simulations, ST-FP HEMT exhibits a good blocking capability compared with HEMT and S-FP HEMT. This benefits from the advantage that the ST-FP could effectively modulate the potential distributions, which could extend the whole electric field distribution between gate and drain and force all the electric field peaks around the gate edge, trench edge and ST-FP edge to be approximately equal but less than breakdown field. Simulations also show that the V_{BR} and η are both weak functions of the trench width L_T and are strong functions of the gate-trench spacing L_{GT}. These results above are of great value for the design and actual manufacture processes of ST-FP HEMTs.

References

[1] Karmalkar S and Mishra U K 2001 *Solid-State Electron.* **45** 1645
[2] Koudymov A, Adivarahan V, Yang J, Simin G and Asif Khan M 2005 *IEEE Electron Dev. Lett.* **26** 704
[3] Brannick A, Zakhleniuk N A, Ridley B K, Shealy J R, Schaff W J and Eastman L F 2009 *IEEE Electron Dev. Lett.* **30** 436
[4] Joh J and del Alamo J A 2006 *IEEE International Electron Devices Meeting*, 2006, San Francisco, CA, USA
[5] Joh J and del Alamo J A 2008 *IEEE Electron Dev. Lett.* **29** 287
[6] Karmalkar S and Mishra U K 2001 *IEEE Trans. Electron Dev.* **48** 1515
[7] Saito W, Takada Y, Kuraguchi M, Tsuda K, Omura I, Ogura T and Ohashi H 2003 *IEEE Trans. Electron Dev.* **50** 2528
[8] Xing H, Dora Y, Chini A, Heikman S, Keller S and Mishra U K 2004 *IEEE Electron Dev. Lett.* **25** 161
[9] Saito W, Kuraguchi M, Takada Y, Tsuda K, Omura I and Ogura T 2005 *IEEE Trans. Electron Dev.* **52** 106
[10] Saito W, Nitta T, Kakiuchi Y, Saito Y, Tsuda K, Omura I and Yamaguchi M 2008 *IEEE Electron Dev. Lett.* **29** 8
[11] Pei Y, Chen Z, Brown D, Keller S, Denbaars S P and Mishra U K 2009 *IEEE Electron Dev. Lett.* **30** 328
[12] Mao W, Yang C, Hao Y, Ma X H, Wang C, Zhang J C, Liu H X, Bi Z W, Xu S R, Yang L A, Yang L, Zhang K, Zhang N Q and Pei Y 2011 *Chin. Phys. B* **20** 097203
[13] Deguchi T, Kamada A, Yamashita M, Tomita H, Arai M, Yamasaki K and Egawa T 2012 *Electron. Lett.* **48** 109
[14] Adak S, Swain S K, Singh A, Pardeshi H, Pati S K and Sarkar C K 2014 *Phys. E.* **64** 152
[15] Zhang P, Zhao S L, Hou B, Wang C, Zheng X F, Ma X H, Zhang J C and Hao Y 2015 *Chin. Phys. B* **24** 037304
[16] Saito W, Suwa T, Uchihara T, Naka T and Kobayashi T 2015 *Microelectron Reliab.* **55** 1682
[17] Onodera H, Hanawa H and Horio K 2016 *Phys. Status Solidi. C* **13** 350
[18] Mao W, She W B, Yang C, Zhang J F, Zheng X F, Wang C and Hao Y 2016 *Chin. Phys. B* **25** 017303
[19] Zhao S L, Wang Y, Yang X L, Lin Z Y, Wang C, Zhang J C, Ma X H and Hao Y 2014 *Chin. Phys. B* **23** 097305
[20] Shealy J R, Prunty T R, Chumbes E M and Ridley B K 2003 *J. Cryst. Growth* **250** 7
[21] Mao W, She W B, Yang C, Zhang C, Zhang J C, Ma X H, Zhang J F, Liu H X, Yang L A, Zhang K, Zhao S L, Chen Y H, Zheng X F and Hao Y 2014 *Chin. Phys. B* **23** 087305
[22] Mao W, Yang C, Hao Y, Zhang J C, Liu H X, Bi Z W, Xu S R, Xue J S, Ma X H, Wang C, Yang L A, Zhang J F and Kuang X W 2011 *Chin. Phys. B* **20** 017203